

See discussions, stats, and author profiles for this publication at: <https://www.researchgate.net/publication/291341940>

Force Sensing by the Vascular Protein Von Willebrand Factor is Tuned by a Strong Intermonomer Interaction

Article in *Proceedings of the National Academy of Sciences* · January 2016

DOI: 10.1073/pnas.1516214113

CITATIONS

3

READS

69

11 authors, including:



Jochen Müller

Ludwig-Maximilians-University of Munich

9 PUBLICATIONS 25 CITATIONS

[SEE PROFILE](#)



Diana Pippig

Ludwig-Maximilians-University of Munich

21 PUBLICATIONS 239 CITATIONS

[SEE PROFILE](#)



Willem Vanderlinden

Ludwig-Maximilians-University of Munich

28 PUBLICATIONS 299 CITATIONS

[SEE PROFILE](#)



Jan Lipfert

Ludwig-Maximilians-University of Munich

96 PUBLICATIONS 2,037 CITATIONS

[SEE PROFILE](#)

Force sensing by the vascular protein von Willebrand factor is tuned by a strong intermonomer interaction

Jochen P. Müller^{a,1}, Salomé Mielke^a, Achim Löf^a, Tobias Obser^b, Christof Beer^a, Linda K. Bruetzel^a, Diana A. Pippig^a, Willem Vanderlinden^{a,c}, Jan Lipfert^a, Reinhard Schneppenheim^b, and Martin Benoit^a

^aDepartment of Physics and Center for Nanoscience, Ludwig Maximilian University of Munich, 80799 Munich, Germany; ^bDepartment of Pediatric Hematology and Oncology, University Medical Center Hamburg-Eppendorf, 20246 Hamburg, Germany; and ^cDepartment of Chemistry, Division of Molecular Imaging and Photonics, KU Leuven–University of Leuven, 3001 Leuven, Belgium

Edited by James A. Spudis, Stanford University School of Medicine, Stanford, CA, and approved December 2, 2015 (received for review August 14, 2015)

The large plasma glycoprotein von Willebrand factor (VWF) senses hydrodynamic forces in the bloodstream and responds to elevated forces with abrupt elongation, thereby increasing its adhesiveness to platelets and collagen. Remarkably, forces on VWF are elevated at sites of vascular injury, where VWF's hemostatic potential is important to mediate platelet aggregation and to recruit platelets to the subendothelial layer. Adversely, elevated forces in stenosed vessels lead to an increased risk of VWF-mediated thrombosis. To dissect the remarkable force-sensing ability of VWF, we have performed atomic force microscopy (AFM)-based single-molecule force measurements on dimers, the smallest repeating subunits of VWF multimers. We have identified a strong intermonomer interaction that involves the D4 domain and critically depends on the presence of divalent ions, consistent with results from small-angle X-ray scattering (SAXS). Dissociation of this strong interaction occurred at forces above ~ 50 pN and provided ~ 80 nm of additional length to the elongation of dimers. Corroborated by the static conformation of VWF, visualized by AFM imaging, we estimate that in VWF multimers approximately one-half of the constituent dimers are firmly closed via the strong intermonomer interaction. As firmly closed dimers markedly shorten VWF's effective length contributing to force sensing, they can be expected to tune VWF's sensitivity to hydrodynamic flow in the blood and to thereby significantly affect VWF's function in hemostasis and thrombosis.

hemostasis | molecular force sensors | protein mechanics | single-molecule force spectroscopy | atomic force microscopy

Force-sensing molecules are critically involved in a variety of biological processes, such as regulation of muscle gene expression or assembly of the cytoskeleton (1–4). In the vasculature, activation of the plasma glycoprotein von Willebrand factor (VWF) for hemostasis crucially depends on its distinct ability to sense hydrodynamic forces (5–7). These forces result from the interplay between hydrodynamic flow and VWF's extraordinary length (8–10), which can exceed $15\ \mu\text{m}$ in the plasma (6). VWF's length arises from its linear multimeric nature. Linear multimers (concatamers) are composed of a variable number of dimers, which are linked N-terminally via disulfide bonds. Dimers, the smallest repeating subunits of VWF with a molecular mass of ~ 500 kDa, consist of two monomers that are linked via C-terminal disulfide bonds (11, 12).

Under static conditions, VWF was reported to adopt a collapsed conformation (6). When subjected to sufficiently high forces, as for instance at sites of vascular injury, vasoconstriction, or stenosis, VWF undergoes an abrupt transition from the collapsed to a stretched conformation (Fig. 14) (6). This transition was shown to correlate with an increased adhesiveness to collagen and platelets (6, 13), enabling stretched VWF to recruit platelets to an injured vessel wall and to promote the formation of a platelet plug. VWF's physiological importance is underlined by mutations that can cause von Willebrand disease (14), the most common hereditary bleeding disorder.

Down-regulation of VWF's hemostatic potential is achieved by the cleavage of long concatamers into shorter ones by the enzyme ADAMTS13 (a disintegrin and metalloprotease with a thrombospondin type 1 motif, member 13) (15). Notably, the specific cleavage site is buried in the A2 domain and exposed by A2 unfolding (8, 16). The interplay of force-induced A2 unfolding and enzymatic cleavage has been investigated in detail at single-molecule level (8). In this context, unfolding of an isolated A2 domain was shown to occur at forces of ~ 7 – 14 pN at loading rates ranging from 0.35 to $350\ \text{pN}\cdot\text{s}^{-1}$. In the presence of neighboring A1 and A3 domains, A2 unfolding was observed at slightly higher forces of ~ 20 pN and comparable loading rates (17).

VWF's activation for hemostasis correlates with its elongation above a critical force threshold (6, 7). However, the current understanding of the underlying molecular mechanisms is limited. Clearly, A2 unfolding is likely to contribute significantly to the elongation of VWF, as the induced length increment of roughly 45 nm (at 20 pN) is almost as large as the end-to-end length of a static monomer (8, 17–19). Stabilization of all other domains in VWF through disulfide bonds was predicted (20), but lacks experimental evidence.

Besides domain unfolding, separation of potential intramonomer and intermonomer interactions may play a crucial role for VWF's elongation. For example, interactions between monomers may tune VWF's force-sensing ability by promoting compactness, as suggested by various computational studies (6, 21, 22). Experimentally, self-association of VWF molecules was reported, but has not been assigned to individual domains (23, 24).

Significance

Excessive blood loss at a site of vascular injury is prevented by recruitment of platelets to the injured vessel wall and the formation of a platelet plug. Under elevated shear flow conditions, these processes are critically mediated by the large plasma glycoprotein von Willebrand factor (VWF). Remarkably, VWF's activation for hemostasis correlates with its abrupt elongation at sufficiently high shear rates. In this study, we have discovered a strong intermonomer interaction in VWF that is expected to tune VWF's ability to sense hydrodynamic forces in the bloodstream. Our data will help to comprehend the force-induced activation of VWF and provide clues for understanding clotting disorders, such as von Willebrand disease and thrombosis, at the single-molecule level.

Author contributions: J.P.M., R.S., and M.B. designed research; J.P.M., S.M., A.L., C.B., and L.K.B. performed research; T.O. and D.A.P. engineered recombinant proteins; J.P.M., S.M., A.L., C.B., L.K.B., W.V., and J.L. analyzed data; and J.P.M. wrote the paper with input from coauthors.

The authors declare no conflict of interest.

This article is a PNAS Direct Submission.

Freely available online through the PNAS open access option.

¹To whom correspondence should be addressed. Email: jochen.mueller@physik.uni-muenchen.de.

This article contains supporting information online at www.pnas.org/lookup/suppl/doi:10.1073/pnas.1516214113/-DCSupplemental.

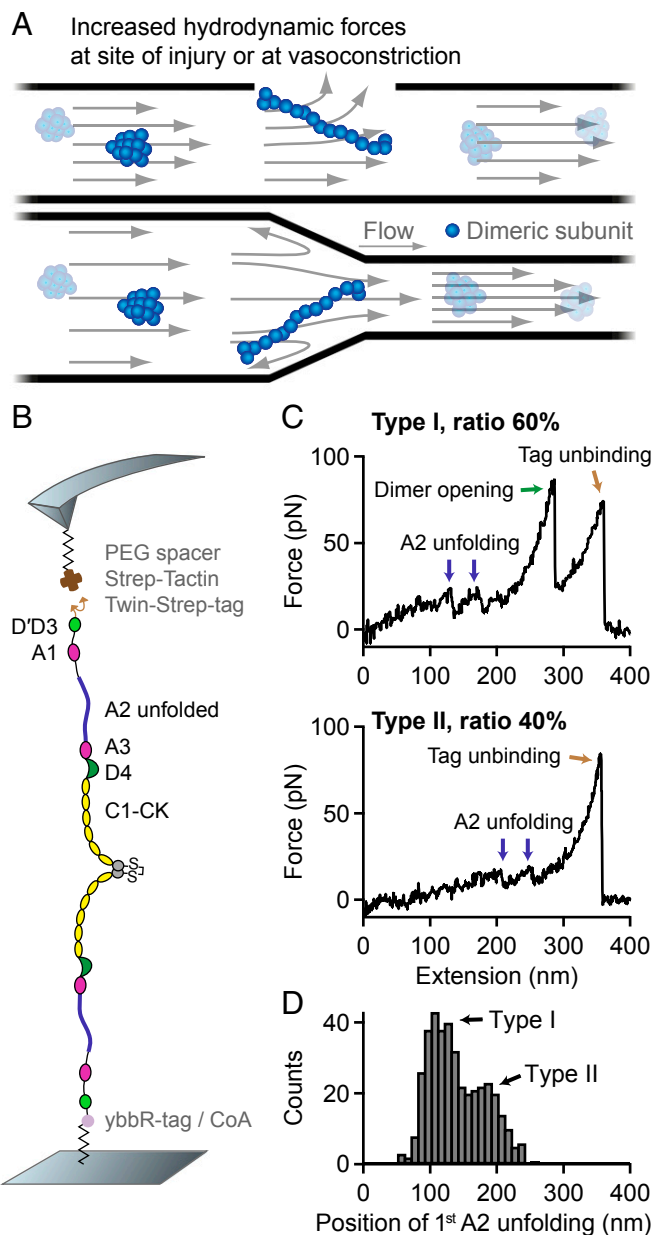


Fig. 1. Single-molecule force measurements on VWF dimers. (A) Illustration of VWF's ability to sense hydrodynamic forces in blood vessels. When subjected to sufficiently high forces, for instance at sites of vascular injury, vasoconstriction, or stenosis, VWF undergoes an abrupt transition from a collapsed to a stretched conformation and promotes hemostasis. (B) Schematic representation of pulling recombinant VWF dimers. A ybbR-tag at the N terminus of one of the monomers allowed for covalent anchoring, and a Twin-Strep-tag at the N terminus of the other monomer enabled specific pulling via a Strep-Tactin functionalized AFM cantilever. (C) Denoised force-extension traces of dimers showing A2 unfolding peaks (blue arrows) at low (type I traces) or at high extension values (type II traces). Type I traces repeatedly exhibited a peak (dimer opening, green arrow) at higher force. The final peak (brown arrow) corresponds to the unbinding of the Twin-Strep-tag from Strep-Tactin. (D) Bimodal distribution of the position of the first A2 unfolding event.

In this study, we report on force-induced conformational changes of VWF and present a strong intermonomer interaction that is expected to tune VWF's force-sensing ability in the bloodstream. Evidence for this interaction comes from force-extension traces of dimers, which were probed in atomic force microscopy (AFM)-based single-molecule force measurements. Complementarily, we

characterized the static conformation of VWF by AFM imaging and small-angle X-ray scattering (SAXS). From the combination of force and imaging data, we gain a quantitative understanding of the mechanisms underlying the force-sensing ability of VWF.

Results

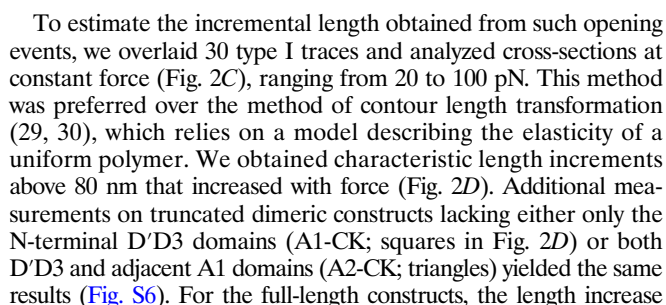
Force Response of VWF Dimers. For AFM-based single-molecule force experiments, we genetically engineered VWF heterodimers, composed of two monomers with different peptide tags (Fig. 1B). These tags were located at the N termini of constituent monomers, thus allowing for pulling VWF in its native force-sensing direction. A ybbR-tag at the end of one of the monomers enabled covalent anchoring to a Coenzyme A (CoA) functionalized glass surface (25), and a Twin-Strep-tag at the end of the other monomer allowed for specific pulling via a Strep-Tactin functionalized AFM cantilever (26). The Twin-Strep-tag was preferred over a single Strep-tag to achieve more stable binding and reduced off-rates. To minimize protein-surface interaction, polyethylene glycol (PEG) spacers were used both at glass surface and cantilever (*Materials and Methods*).

Force-extension traces of specific pulling events were identified by using the characteristic unfolding pattern of the A2 domain as a positive fingerprint (Fig. 1C). Due to the existence of two A2 domains in dimers, only traces with two A2 unfolding peaks were considered. We verified that this fingerprint corresponds to A2 unfolding by pulling heterodimers with disulfide bridged A2 domains (Fig. S1) and by pulling bifunctional monomers (Fig. S2). Characteristic peak forces on the order of 20 pN and subsequent length increments of ~45 nm are in agreement with reported values for A2 unfolding (8, 17–19). Moreover, forces of the last peak (rupture peak) in force-extension traces are in line with those reported for dissociating the Strep-tag/Strep-Tactin interaction (27), underlining the specific nature of the analyzed pulling events (Fig. S3).

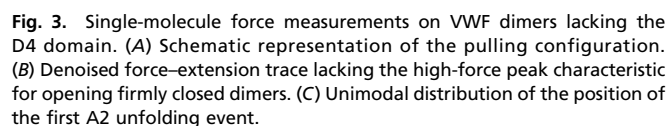
We obtained two types of force-extension traces of VWF dimers under near-physiological buffer conditions (Fig. 1C and Fig. S4), showing A2 unfolding peaks at low (type I) and at high extension values (type II). Type II traces revealed the first A2 unfolding peak at extension values of 179 ± 29 nm and the second A2 unfolding peak at 226 ± 37 nm. Given a static end-to-end length of ~130 nm for a VWF dimer and an overall linker length of 60 nm, these traces are in line with expectations for loading a flexible (open) dimer (28). Traces of type I showed A2 unfolding peaks at considerably lower extension values of 110 ± 22 nm (first A2) and 161 ± 22 nm (second A2). Classification of traces into two types is backed up by a bimodal distribution of the position of both first (Fig. 1D) and second A2 unfolding. From a double-Gaussian fit to the distribution of the first A2 unfolding position, we estimated the ratio of type I traces as 60% and type II traces as 40%.

In traces of type I, we repeatedly observed an additional high-force peak (green arrow in Fig. 1C) before the rupture peak. In these cases, the position of rupture closely matched the one observed in type II traces. However, as a result of the relatively weak Twin-Strep-tag/Strep-Tactin interaction, this additional peak only showed up in ~10% of type I traces. In the remaining 90% of type I traces, rupture of the construct from the cantilever occurred before observing a high-force peak, and at considerably lower extension values (Fig. S5).

The high-force peak was observed at forces ranging from roughly 50–120 pN, depending on the applied loading rate (Fig. 2B). Importantly, the high-force peak was never observed twice in a trace and, moreover, was never observed in monomer traces (Fig. S2). Consequently, we excluded domain unfolding as the origin of this high-force peak, in agreement with the prediction of disulfide bonds stabilizing all domains in VWF except the A2 domain (20). Hence, we hypothesized this peak to result from the dissociation of a strong intermonomer interaction, which may be conceptualized as the opening of a firmly closed dimer (Fig. 24).



Static Conformation of VWF. By AFM imaging, we visualized the static conformation of dimeric VWF constructs (Fig. 4 and Figs. S10–S12), adsorbed from near-physiological buffer onto a poly-L-lysine-coated mica surface. We found dimers with conformations ranging from fully flexible to fully closed (Fig. 4A). To quantify the compactness of a dimer, we measured its stem length, i.e., the distance from the CK domain to the position at which the two constituent monomers separate from each other. Additionally, we determined the distance between the CK domain and the beginning of higher N-terminal domains for the two constituent monomers and used the mean of these distances to normalize the stem length (Fig. S10). For wild-type dimers, the distribution of the normalized stem length (Fig. 4B) yielded one peak decaying from zero stem length (flexible dimers, ~65%), and another peak centered slightly above 1 (closed dimers, ~35%). Dimers lacking the D4 domain (Fig. 4C) and full-length dimers adsorbed from buffer containing EDTA (Fig. S9) exhibited only the population of normalized stem



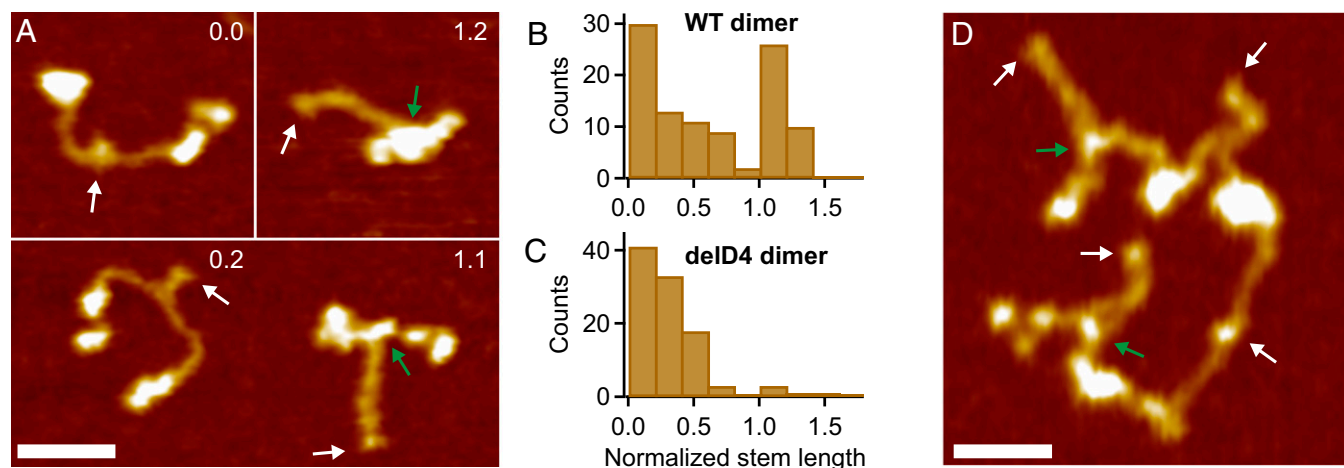


Fig. 4. Static conformation of VWF probed by AFM imaging. (A) Images of individual VWF dimers. Conformations of dimers range from fully flexible (normalized stem length of 0) to fully closed (normalized stem length above 1). Numbers in images are values of the normalized stem length. White arrows mark the CK domains, and green arrows mark positions corresponding to potential strong intermonomer interactions. (Scale bar, 30 nm; range of color scale, 2.4 nm.) (B) Distribution of the normalized stem length of wildtype (WT) dimers, showing a peak decaying from zero stem length and a peak centered slightly above 1. (C) Distribution of the normalized stem length of dimers lacking the D4 domain, showing only the peak decaying from zero stem length. (D) Image of a VWF concatamer consisting of four dimeric subunits. Arrows and scales are as in A.

lengths decaying from zero (Fig. 4C and Fig. S9). The observed stem length distributions are consistent with a simple model assuming C domains to zip up pairwise from the CK domains with a constant domain–domain interaction free energy (Fig. S11). This model suggests that forces in the low piconewton range—below the force resolution of AFM force measurements—are sufficient to break C-domain interactions.

Additionally, we probed the conformation of dimeric VWF constructs (A1–CK) in solution using SAXS (*Supporting Information*). The SAXS data indicate a change in the conformational ensemble from relatively rigid conformations under near-physiological buffer conditions to more flexible and as a result more globular conformations in the presence of EDTA (Fig. S9), fully consistent with the AFM results.

AFM imaging further revealed that dimers as constituents of concatamers (Fig. 4D) exhibit similar static conformations and a similar degree of compactness as isolated ones. Especially in multimeric samples, we also observed dimers exhibiting colocalization of N-terminal portions of the constituent monomers, likely resulting from the strong intermonomer interaction, despite not possessing a fully closed stem (lower left dimer in Fig. 4D). Importantly, we did not observe any clear colocalization between distinct dimers within a concatamer except the intrinsic multimerization through D'D3.

Discussion

In this study, we used AFM-based single-molecule force measurements to probe the force response of VWF dimers. We identified a strong intermonomer interaction that withstood forces of 50–120 pN at loading rates ranging from 0.1 to 10 nN·s^{−1}. For each loading rate, the measured forces presumably represent only the lower part of a distribution of forces required for dissociating the strong intermonomer interaction. This bias is a result of the relatively weak Twin-Strep-tag/Strep-Tactin interaction, which was used for pulling VWF and dissociates at forces that are in a similar range as those of the strong intermonomer interaction. It is therefore likely that the force-loading-rate dependency of the dissociation of the strong intermonomer interaction is characterized by higher mean forces than measured in our experiments.

The strong intermonomer interaction appears to be highly specific, judging from a reproducible length increase after dissociation. Additionally, the interaction was only observed in the presence of

divalent ions. These results are corroborated by observations from AFM imaging, which revealed both compact and flexible conformations of VWF dimers at pH 7.4 in the presence of divalent ions, but only flexible conformations upon addition of EDTA. This finding is in line with previous transmission electron microscopy (TEM) studies on VWF at pH 7.4 in absence of divalent ions (28, 33). Further evidence for a specific intermonomer interaction comes from experiments on deletion constructs. While deletion of the A3 domain did not significantly change the force response of VWF dimers, the strong intermonomer interaction disappeared upon deletion of the D4 domain. This finding is again supported by AFM imaging, which showed that deletion of D4 promotes a flexible conformation of dimers. Recent TEM studies showed that a D4–D4 complex forms at pH 6.2 in the presence of calcium and promotes stem formation (28). We hypothesize that a D4–D4 complex also forms under physiological conditions, explaining our force and imaging data.

Force–extension traces of firmly closed dimers are characterized by A2 unfolding peaks at low extension values. Flexible dimers, such as induced by addition of EDTA, show A2 unfolding peaks at considerably higher extension values. Under near-physiological buffer conditions, we found two populations in the positions of first and second A2 unfolding events. A rough estimation based on a double-Gaussian fit yielded a ratio of 60% firmly closed and 40% flexible dimers. The existence of firmly closed and flexible dimers is corroborated by AFM imaging results, although quantified with roughly inverted ratios (35% closed, 65% flexible). The difference in ratios may well originate both from uncertainties of the double-Gaussian fit and from the strict criterion of a fully formed stem for assigning dimers as compact. Remarkably, the observed ratio of approximately one-half firmly closed and one-half flexible dimers indicates a difference in Gibbs free energy close to zero between the firmly closed and the open state. Given the fact that the dimer bond is mechanically strong, this implies that the exchange kinetics between the two states are exceptionally slow, at least along the reaction coordinate probed in our force measurements. For elucidating the underlying structural mechanisms, high-resolution structures of the D4 domain and of the C domains are of outstanding interest. AFM imaging further revealed that dimers within VWF concatamers have a similar conformation as isolated ones. In particular, we found flexible and closed dimers with very similar ratios. As we did not observe any clear colocalization

18. Jakobi AJ, Mashaghi A, Tans SJ, Huizinga EG (2011) Calcium modulates force sensing by the von Willebrand factor A2 domain. *Nat Commun* 2:385.
19. Xu AJ, Springer TA (2012) Calcium stabilizes the von Willebrand factor A2 domain by promoting refolding. *Proc Natl Acad Sci USA* 109(10):3742–3747.
20. Zhou Y-F, et al. (2012) Sequence and structure relationships within von Willebrand factor. *Blood* 120(2):449–458.
21. Alexander-Katz A, Schneider MF, Schneider SW, Wixforth A, Netz RR (2006) Shear-flow-induced unfolding of polymeric globules. *Phys Rev Lett* 97(13):138101.
22. Alexander-Katz A (2014) Toward novel polymer-based materials inspired in blood clotting. *Macromolecules* 47(5):1503–1513.
23. Savage B, Sixma JJ, Ruggeri ZM (2002) Functional self-association of von Willebrand factor during platelet adhesion under flow. *Proc Natl Acad Sci USA* 99(1):425–430.
24. Ulrichs H, et al. (2005) The von Willebrand factor self-association is modulated by a multiple domain interaction. *J Thromb Haemost* 3(3):552–561.
25. Yin J, et al. (2005) Genetically encoded short peptide tag for versatile protein labeling by Sfp phosphopantetheinyl transferase. *Proc Natl Acad Sci USA* 102(44):15815–15820.
26. Schmidt TGM, et al. (2013) Development of the Twin-Strep-tag® and its application for purification of recombinant proteins from cell culture supernatants. *Protein Expr Purif* 92(1):54–61.
27. Kim M, Wang CC, Benedetti F, Marszalek PE (2012) A nanoscale force probe for gauging intermolecular interactions. *Angew Chem Int Ed Engl* 51(8):1903–1906.
28. Zhou Y-F, et al. (2011) A pH-regulated dimeric bouquet in the structure of von Willebrand factor. *EMBO J* 30(19):4098–4111.
29. Puchner EM, Franzen G, Gautel M, Gaub HE (2008) Comparing proteins by their unfolding pattern. *Biophys J* 95(1):426–434.
30. Stahl SW, et al. (2012) Single-molecule dissection of the high-affinity cohesin–dock-erin complex. *Proc Natl Acad Sci USA* 109(50):20431–20436.
31. Bustamante C, Marko JF, Siggia ED, Smith S (1994) Entropic elasticity of lambda-phage DNA. *Science* 265(5178):1599–1600.
32. Odijk T (1995) Stiff chains and filaments under tension. *Macromolecules* 28:7016–7018.
33. Fowler WE, Fretto LJ, Hamilton KK, Erickson HP, McKee PA (1985) Substructure of human von Willebrand factor. *J Clin Invest* 76(4):1491–1500.
34. Sing CE, Alexander-Katz A (2010) Elongational flow induces the unfolding of von Willebrand factor at physiological flow rates. *Biophys J* 98(9):L35–L37.
35. Steppich DM, et al. (2008) Relaxation of ultralarge VWF bundles in a microfluidic-AFM hybrid reactor. *Biochem Biophys Res Commun* 369(2):507–512.
36. Lipfert J, Doniach S (2007) Small-angle X-ray scattering from RNA, proteins, and protein complexes. *Annu Rev Biophys Biomol Struct* 36:307–327.
37. Putnam CD, Hammel M, Hura GL, Tainer JA (2007) X-ray solution scattering (SAXS) combined with crystallography and computation: Defining accurate macromolecular structures, conformations and assemblies in solution. *Q Rev Biophys* 40(3):191–285.
38. Svergun DI, Koch MHJ (2003) Small-angle scattering studies of biological macromolecules in solution. *Rep Prog Phys* 66:1735–1782.
39. Doniach S (2001) Changes in biomolecular conformation seen by small angle X-ray scattering. *Chem Rev* 101(6):1763–1778.
40. Zimmermann JL, Nicolaus T, Neuert G, Blank K (2010) Thiol-based, site-specific and covalent immobilization of biomolecules for single-molecule experiments. *Nat Protoc* 5(6):975–985.
41. Gump H, Stahl SW, Strackharn M, Puchner EM, Gaub HE (2009) Ultrastable combined atomic force and total internal reflection fluorescence microscope. *Rev Sci Instrum* 80(6):063704.
42. Hutter JL, Bechhoefer J (1993) Calibration of atomic-force microscope tips. *Rev Sci Instrum* 64:1868–1873.
43. Condat L (2013) A direct algorithm for 1-D total variation denoising. *IEEE Signal Process Lett* 20:1054–1057.
44. Vanderlinden W, et al. (2012) Mesoscale DNA structural changes on binding and photoreaction with Ru[(TAP)₂PHEHAT]²⁺. *J Am Chem Soc* 134(24):10214–10221.
45. Blanchet CE, et al. (2015) Versatile sample environments and automation for biological solution X-ray scattering experiments at the P12 beamline (PETRA III, DESY). *J Appl Cryst* 48(Pt 2):431–443.
46. Konarev PV, Volkov VV, Sokolova AV, Koch MHJ, Svergun DI (2003) PRIMUS: A Windows PC-based system for small-angle scattering data analysis. *J Appl Cryst* 36:1277–1282.
47. Rivetti C, Guthold M, Bustamante C (1996) Scanning force microscopy of DNA deposited onto mica: Equilibration versus kinetic trapping studied by statistical polymer chain analysis. *J Mol Biol* 264(5):919–932.
48. Wen D, Foley SF, Hronowski XL, Gu S, Meier W (2013) Discovery and investigation of O-xylosylation in engineered proteins containing a (GGGG)_n linker. *Anal Chem* 85(9):4805–4812.
49. Spahr C, et al. (2013) Recombinant human lecithin-cholesterol acyltransferase Fc fusion: Analysis of N- and O-linked glycans and identification and elimination of a xylose-based O-linked tetrasaccharide core in the linker region. *Protein Sci* 22(12):1739–1753.
50. Spencer D, et al. (2013) O-xylosylation in a recombinant protein is directed at a common motif on glycine-serine linkers. *J Pharm Sci* 102(11):3920–3924.
51. Spahr C, Shi SD-H, Lu HS (2014) O-glycosylation of glycine-serine linkers in recombinant Fc-fusion proteins: Attachment of glycosaminoglycans and other intermediates with phosphorylation at the xylose sugar subunit. *MAbs* 6(4):904–914.